Theoretical calculation of Penning-ionization cross sections for collisions of He($2^{1,3}S$) with sodium atoms

James S. Cohen and Richard L. Martin
Theoretical Division, Los Alamos National Laboratory, Los Alamos, New Mexico 87545

Neal F. Lane
Physics Department and Rice Quantum Institute, Rice University, Houston, Texas 77251

(Received 11 June 1984)

Cross sections have been calculated for the Penning ionization of ground-state sodium atoms in collisions with metastable He($2^{1,3}S$) atoms for the range of center-of-mass energies 0.01 eV $\leq E \leq 1.0$ eV. The cross sections were calculated with use of optical-model potentials. The real parts of the relevant potential-energy curves were determined by carrying out a configuration-interaction (CI) calculation on the NaHe molecule. The potentials were adjusted to yield the correct asymptotic van der Waals form. The imaginary parts of the potentials correspond to autoionization rates and were obtained from a Stieltjes moment analysis of a discrete (L^2) representation of the $e^- + \mathrm{NaHe}^+$ continuum, as represented by diffuse molecular orbitals generated by the CI procedure. The calculated cross section for He(2^3S) on Na at $E=0.04$ eV is in good agreement with stationary-afterglow measurements at room temperature. The singlet-to-triplet ratio of cross sections is in good agreement with that measured by beam techniques. Elastic differential cross sections for He(2^1S) scattered from Na have also been calculated. Satisfactory agreement is obtained with recent crossed-beam measurements.

I. INTRODUCTION

Slow collisions between atoms or ions are generally adiabatic, and do not result in electronic transitions unless near-degeneracy is present between the initial and final electronic states at an internuclear separation realized during the collision. Avoided crossings ("pseudocrossings") of potential curves can provide the necessary near-degeneracy for electronic transitions between bound atomic states.[1,2] However, in a collision between an excited atom A^* with excitation energy E_A and an atom B with ionization energy I_B, a "bound-free" electronic transition is possible as long as $E_A \geq I_B$, resulting in the Penning-ionization (PI) process

$$A^* + B \rightarrow A + B^+ + e^- , \tag{1}$$

which may also be thought of as excitation transfer to the continuum.[3-6] Since the energy E of the outgoing electron lies in a continuum of values it is possible to have exact energy degeneracy between initial and final electronic states at all internuclear separations accessible during the collision. Thus, it is not surprising that PI cross sections at thermal energies are found to be large for a wide variety of systems. If the positive ion AB^+ is bound, then associative ionization (AI) is possible, in which the electron carries away sufficient energy to leave the molecular ion bound in a rovibrational state j,v according to the AI process

$$A^* + B \rightarrow AB^+(j,v) + e^- . \tag{2}$$

Most PI reactions that have been studied to date involve the long-lived metastable species He(2^3S) and He(2^1S). Since the excitation energies $E(2^3S)=19.8$ eV and $E(2^1S)=20.6$ eV exceed the first ionization energies of all atoms and molecules other than He and Ne, Penning ionization is generally possible. Experimental ionization rates, usually at room temperature, have been determined for a large number of species by means of afterglow techniques, and some cross sections have been measured in beam experiments.[3-6] Application of the theory to PI and/or AI reactions is difficult in practice,[7-9] and very few *ab initio* calculations have been performed.[10-13] Even in the adiabatic theory, generally valid for slow collisions, one must calculate the electronic energy and wave function describing the initial $A^* + B$ "resonance" molecular state, which is unstable with respect to autoionization (i.e., PI and/or AI), as well as the transition matrix elements that involve the continuum-state wave function for $A + B^+ + e^-$.

The present study of Penning ionization of Na by He($2^{1,3}S$) was motivated in part by the stationary-afterglow measurements of Johnson *et al.*[14] in which thermal-velocity ionization rates (with a quoted uncertainty of $\pm 20\%$) were determined for collisions of He(2^3S) atoms with alkali-metal atoms. The average cross sections extracted from these rates are $(33\pm6)\times10^{-16}$, $(55\pm10)\times10^{-16}$, $(93\pm18)\times10^{-16}$, and $(34\pm7)\times10^{-16}$ cm^2 for Na, K, Rb, and Cs, respectively. The result for Cs has since been confirmed by Tolmachev and Fogel.[15] The relatively small cross section observed for Cs is in sharp contrast with the trend of Na, K, and Rb. Johnson *et al.* speculate that the ionization rate measured for K and Rb may include important contributions from indirect processes such as

$$\mathrm{He}(2^3S)+\mathrm{K}(3p^6 4s)\rightarrow \mathrm{He}(1^1S)+\mathrm{K}(3p^5 4snl)\ , \quad (3)$$

where the final "core-excited" atomic state of K is itself unstable with respect to autoionization. Since it is the destruction rate of $\mathrm{He}(2^3S)$ atoms that is measured, transitions to core-excited atomic autoionizing states, as in (3), would also be included. Johnson *et al.* point out that Rydberg series of such states exist, some members of which are nearly degenerate with the initial electronic energy of $\mathrm{He}(2^3S)$ and ground-state K or Rb. For Na, the energies of these core-excited states lie 10—20 eV too high to be involved; and for Cs, the whole series, corresponding to configurations $\mathrm{Cs}(5p^5 6snl)$, lies ~ 5 eV below the initial electronic energy of the system, and therefore out of resonance. Of course there are other series of core-excited states of Cs that could be involved. Moreover, the first excited state of Cs^+ is energetically accessible, and this additional channel should make a contribution to the total ionization cross section. Nevertheless, the observed trend is clear; and the interpretation raises interesting basic questions about the nature of nonadiabatic interactions between two characteristically different classes of electronic states, each unstable with respect to autoionization. This is not an issue for the present study of Penning ionization of Na by $\mathrm{He}(2^{1,3}S)$ atoms. The purpose of this work is to demonstrate that calculations of PI and/or AI for multielectron systems are feasible, using modern L^2 techniques to avoid the awkward electronic continuum calculations. The success of the present work encourages us to extend the study to K in the future so that the role of the core-excited atomic autoionization states can be explicitly examined.

The organization of the paper is as follows. In Sec. II we present a brief description of the theoretical basis of the optical model as it applies to PI and/or AI, and the definitions of the real and imaginary ("width") parts of the potential and the cross sections. In Sec. III the molecular-structure calculations are described, as well as the Stieltjes moment procedure used to determine the width function. In Sec. IV the calculated PI cross sections are described and discussed. Finally, in Sec. V, the calculated elastic differential cross sections for $\mathrm{He}(2^1S)$ on Na are discussed and compared with semiempirical results.

II. THEORETICAL BACKGROUND

The theory of Penning and associative ionization has been described by Nakamura[7] and by Miller.[8] The latter approach is based on an application of Feshbach's projection-operator formalism to the determination of resonance electronic states of the system in the context of the Born-Oppenheimer approximation, and is very similar to O'Malley's formulation[16] of the dissociative-attachment problem. Since we are concerned with very slow collisions ($v_{\mathrm{rel}} \ll 1$ a.u.), nonadiabatic corrections to the Born-Oppenheimer approximation should be negligible, except for possible pseudocrossings that may occur for some systems (e.g., the core-excited atomic autoionization states described earlier). In such cases, the nonabiabatic coupling is likely to be localized to a narrow range of internuclear separations, and standard methods may be applicable with only slight variations. In the present application to Na, there are no pseudocrossings to concern us.

Thus, following Feshbach's definition of the resonance state,[17] the electronic Hilbert space is partitioned by means of projection operators P and Q, where the latter projects onto the resonance states (autoionizing states NaHe^*, in our application), and $P=1-Q$ projects onto all other states (the $e^-+\mathrm{NaHe}^+$ continuum, in our application). For each energy E and internuclear separation R, the exact electronic wave function can be written

$$\psi_E=(P+Q)\psi_E=P\psi_E+Q\psi_E\ , \quad (4)$$

where $P\psi_E$ and $Q\psi_E$ satisfy complicated coupled equations. The practical importance of the procedure lies in the validity of an approximation procedure in which one ignores the coupling to zeroth order and defines approximate representations of the resonance function

$$\phi_r \simeq Q\psi_E\ , \quad (5)$$

satisfying a (bound) eigenvalue equation

$$(QHQ-E_r)\phi_r=0\ , \quad (6)$$

and the background continuum function

$$\chi_E \simeq P\psi_E\ , \quad (7)$$

which satisfies a continuum eigenvalue equation

$$(PHP-E)\chi_E=0\ . \quad (8)$$

If one takes into account the coupling between the approximate resonance and continuum states, the resonance-state eigenvalue becomes

$$E_r'=E_r+\Delta-\frac{i}{2}\Gamma\ , \quad (9)$$

where the shift Δ, being small relative to E_r, is usually ignored, and where the width is given by the expression

$$\Gamma=2\pi\rho_E\,|\,\langle\chi_E\,|\,(H-E)\,|\,\phi_r\rangle\,|^2\ , \quad (10)$$

involving the density of states ρ_E dictated by the normalization of χ_E. Choosing the best resonance function ϕ_r is something of an art. In the present application we utilize the similarity of the NaHe molecular orbitals to those of the separated atoms to associate the resonance with the roots of a limited CI wave function in which the $1s$ orbital of helium is singly occupied.

One can gain some appreciation for the appropriateness of this approximation to the Feshbach description by recalling the physical nature of the resonance state. If we form a wave packet by superimposing stationary-state wave functions [from Eq. (4)] allowing a small spread in electronic energy E about E_r (and of course a corresponding spread in momentum $\vec{k}$ of the continuum electron), we can write

$$\psi(t)=P\psi(t)+Q\psi(t)\ . \quad (11)$$

Now, at times $t\rightarrow-\infty$, $P\psi_E(t)$ represents a "free-electron" wave packet incident on the ion (in our case NaHe^+ at a fixed R). As the electron's wave packet begins to overlap the electronic orbitals of the target ion, say

as $t \to 0$, there is a finite probability for one of the target electrons, (e.g., the $1s$ orbital of a perturbed He) to be excited (e.g., to the $2s$ orbital of a perturbed He) while the incident electron is temporarily trapped in another available orbital (e.g., the $3s$ orbital of a perturbed Na). Roughly, the process may be described by

$$[e^- + \mathrm{He}(1s^2)\mathrm{Na}^+]_P \leftrightarrows [\mathrm{He}(1s\,2s)\mathrm{Na}(3s)]_Q \ , \quad (12)$$

where the P,Q subscripts remind us that the transient excitation to HeNa* is contained in $Q\psi(t)$, and corresponds to a growth in the amplitude of this part of the wave function and a corresponding reduction in the amplitude of $P\psi(t)$ at $t \approx 0$. Of course, as $t \to +\infty$, $Q\psi(t)$ again falls to zero, and the outgoing electron's wave packet is contained in $P\psi(t)$. The inverse of "width," Γ^{-1}, gives the decay time (in a.u.) of the resonance. Now, referring to Eq. (11), it is clear that for $t \approx 0$, i.e., for the incident electron close to the ion, $\psi(t)$ is dominated by $Q\psi(t)$, and small errors in $P\psi(t)$ are unimportant. The excitation of $P\psi(t)$ for $t > 0$ is dominated by what is "fed in" from $Q\psi(t)$. Thus it is essential that in this region of configuration space (i.e., "close in") we have a good representation of the resonance wave function. Returning to the stationary-state description and Eq. (5), we conclude that ϕ_r must be a good representation of $Q\psi_E$ in the close-in region. Miller has argued this directly from the time-independent formalism.[18]

The nuclear motion is determined by the adiabatic response of the electrons to the instantaneous nuclear field. Thus the nuclear Schrödinger equation is

$$\left[-\frac{1}{2\mu}\nabla_R^2 + W_r(R) - E_n\right]\psi_{\mathrm{nuc}}(\vec{R}) = 0 \ , \quad (13)$$

where the nuclear potential energy is defined in terms of the resonance electronic energy and width by the optical potential

$$W_r(R) = E_r(R) - E_r(\infty) - \tfrac{1}{2}i\Gamma(r) + 22/R \ , \quad (14)$$

and where E_n is the center-of-mass nuclear kinetic energy. Since the initial electronic state corresponds to $\mathrm{He}(2^{1,3}S) + \mathrm{Na}$, it is assumed that for slow nuclear motion the electronic energy will follow the adiabatic curve. However, autoionization is possible at all finite R and leads to a flux loss ("absorption") from the nuclear elastic channel; the imaginary term in $W_r(R)$ takes this into account. The absorption cross section describes Penning ionization and is given in terms of the imaginary parts of the complex phase shifts

$$\eta_l = \eta_l^R + i\eta_l^I \quad (15)$$

by the standard expression

$$\sigma_{\mathrm{ion}}(E) = g(\pi/k^2)\sum_{l=0}^{\infty}(2l+1)[1 - \exp(-4\eta_l^I)] \ , \quad (16)$$

where k is related to the center-of-mass nuclear kinetic energy by

$$k^2 = 2\mu E_n \ , \quad (17)$$

$\mu = 6214$ is the reduced nuclear mass (in a.u.), and $g = 1$ for $\mathrm{He}(2^1S)$ and $g = \frac{1}{3}$ for He (2^3S); the latter is a statistical weight factor associated with the $^2\Sigma$ state dissociating to $\mathrm{He}(2^3S) + \mathrm{Na}$. The $^4\Sigma$ state is essentially stable, and does not contribute to Penning ionization.

III. MOLECULAR STRUCTURE AND WIDTH DETERMINATION

The electronic problem involves four phases: (1) a spin- and symmetry-restricted Hartree-Fock calculation of the ground state of NaHe; (2) a CI calculation of resonance $^2\Sigma^+$ states of NaHe* dissociating to $\mathrm{He}(2^3S) + \mathrm{Na}$ and $\mathrm{He}(2^1S) + \mathrm{Na}$; (3) calculation of L^2 width matrix elements from the partitioned Hamiltonian; and (4) Stieltjes imaging to get continuum-normalized widths.

The basis chosen for the structure determination was an even-tempered set of Gaussian-type orbitals (GTO) with 10-s and 8-p GTO on He, and 15-s, 12-p, and 3-d GTO on Na.[19] Since the same basis is required to represent the continuum states of $e^- + \mathrm{NaHe}^+$, we included diffuse GTO, the smallest orbital exponents being 0.0023, 0.0009, and 0.0275 for s, p, and d orbitals, respectively, on Na, and 0.0017 for s and p orbitals on He. Since only Σ states are of interest in the PI study, certain orbitals, e.g., p_π, d_π, and d_δ, were ignored, except for those required for description of the $2p$ core of Na. The CI calculation included only single excitations with respect to the Hartree-Fock ground state (this resulted in 113 spatial configurations and 187 spin eigenfunctions). This approach ensures a "frozen-core" Hartree-Fock approximation to the $e^- + \mathrm{NaHe}^+$ continuum, and also generates the set of configurations expected to be most important for describing the resonance states, i.e., those resembling $\{\mathrm{He}(1sns)\mathrm{Na}(3s)\}$. Table I compares atomic energies with experimental values. Note that the theoretical results for the Na Rydberg series are in much better agreement with experiment than the He excitation energies. This is not due to a poorer GTO basis for He; rather it reflects the relative appropriateness of the frozen-core approximation for $\mathrm{Na}(nl)$ versus $\mathrm{He}(1snl)$. The fact that the He excitation energies are in fair agreement with experiment is

TABLE I. Atomic excitation energies calculated from the dissociation limits of the CI electronic energies for NaHe (given in eV relative to the ground states).

	Helium			Sodium	
	CI	Experimental		CI	Experimental
2^3S	19.82	19.81	$3p$	1.97	2.10
2^1S	20.61	21.13	$4s$	3.06	3.19
2^3P	20.96	21.23	$3d$	3.59	3.62
2^1P	21.22	21.69	$4p$	3.71	3.75

due to the near-cancellation of two contributions not included in our limited CI: relaxation of the $1s$ orbital in the excited states (which would decrease the *ab initio* excitation energy), and the differential electron correlation energy between the $1s^2$ and $1snl$ pairs (which would increase the *ab initio* excitation energy).

The *ab initio* well depths for the 2^3S (2^1S) potential surfaces are 0.18 eV (0.14 eV) with corresponding equilibrium distances of $6.5a_0$ ($7.7a_0$). Since the CI calculation limited to single excitations does not include the van der Waals contribution, it is not surprising that the calculated well depths are much smaller than the values 0.74 eV (2^3S) and 0.30 eV (2^1S) inferred from the PI electron-energy distributions measured by Hotop and Niehaus.[20] We feel that the experimentally inferred well depths are likely to be accurate. Therefore, we chose to modify the potential-energy curves to exhibit the correct long-range van der Waals behavior and to have the experimental well depths. The modified potential curves have the form

$$V(R)=[E_r^{\mathrm{CI}}(R)-E_r^{\mathrm{CI}}(\infty)+22/R]f(R) -(C_6/R^6)[1-f(R)] , \tag{18}$$

where the cutoff function is defined as

$$f(R)=\exp[-(R/R_0)^8] , \tag{19}$$

and the parameters R_0 are chosen to obtain the experimental well depths. The values chosen for He(2^3S) and He(2^1S) are $R_0=6.27a_0$ and $8.22a_0$, respectively; the corresponding values of C_6 are 2220 and 3660 a.u., respectively.[21] The equilibrium distances deduced from this fit are then $5.85a_0$ ($7.35a_0$) for the 2^3S (2^1S) surfaces. The classical turning points for thermal collisions are $\gtrsim 4.4a_0$ ($5.7a_0$). In Fig. 1, the resonance potential curves are shown corresponding to the semiempirical modification.

In order to calculate the imaginary part of the optical potential, i.e., the width of Eq. (10), we require a representation of the $e^-+\mathrm{NaHe}^+$ continuum.[22–25] The diffuse GTO were included in the basis set for just this purpose. However, in carrying out the CI calculation we have mixed all configurations, so that the wave functions corresponding to the states that dissociate to He($2^{1,3}S$) have

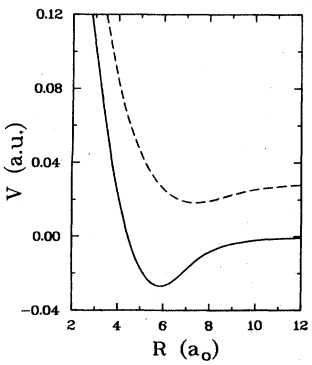

FIG. 1. Potential-energy curves, adjusted to have the correct long-range form. He(2^3S)+Na (solid curve); He(2^1S)+Na (dashed curve).

some contributions for all configurations. Moreover, the CI eigenvectors by definition completely diagonalize the Hamiltonian (i.e., within this CI space). So, if we decided to select some particular eigenvector to represent the continuum in a calculation of the width, the result from Eq. (10) would necessarily be zero. Such a state does not decay into the continuum since it already includes the continuum i.e., it is a representation of the full wave function ψ_E of Eq. (4), not of $Q\psi_E$.

Hazi has described a two-step procedure for separating resonance and continuum states.[22] In the first step, a projection operator Q_0 is defined

$$Q_0=\sum_{j=1}^{N_0} |\chi_j\rangle\langle\chi_j| , \tag{20}$$

where the $|\chi_j\rangle$ are vectors that have features of the desired resonance states. In our case, the $|\chi_j\rangle$ are taken to be Slater determinants corresponding to all singly excited configurations where the molecular orbital corresponding to the $1s$ orbital of He is singly occupied. More precisely, if the ground state of NaHe is denoted as (core) $1\sigma^2 2\sigma$, then all excitations of the form (core) $1\sigma 2\sigma n\sigma$ are included in Q_0. Note that this space includes as a subset all configurations dissociating to He($1snl$)+Na($3s$). The Q_0-space Hamiltonian Q_0HQ_0 is then diagonalized to obtain resonance eigenfunctions $|\psi_i\rangle$ and energies E_i. Next we choose the two lowest-lying resonant states $|\psi_1\rangle$ and $|\psi_2\rangle$ and define a new Q space with

$$Q=\sum_{i=1}^{2} |\psi_i\rangle\langle\psi_i| , \tag{21}$$

where $i=1,2$ label the states dissociating to Na+He(2^3S) and Na+He(2^1S), respectively. The operator $P=1-Q$ now contains all the lower-lying continuum, and the eigenfunctions $|\phi_n\rangle$ of PHP are taken to be representations of the continuum at energies given by the eigenvalues E_n. Thus, we have the matrix elements

$$\gamma_n=2\pi|\langle\phi_n|H|\psi_i\rangle|^2 , \tag{22}$$

defined only at discrete energies E_n. The γ_n are not directly usable as approximate widths since the normalization of the ϕ_n is not that of the desired continuum function χ_E of Eq. (7). However, the Stieltjes imaging procedure corrects this improper normalization by taking explicit account of the density of eigenvalues representing the continuous spectrum.[23,24] The direct relevance of the calculated values of γ_n and E_n is that they are useful in determining moments of the width energy distribution. Thus, if one defines exact negative-power moments

$$S(-k)=\int_{\epsilon_0}^{\infty}\frac{\Gamma(\epsilon')}{(\epsilon')^k}d\epsilon' , \tag{23}$$

it is found that the first few moments are approximated well by

$$\tilde{S}(-k)=\sum_{n=1}^{N}\frac{\gamma_n}{(\epsilon_n)^k} \tag{24}$$

as long as $k \ll N$. The zero of energy chosen in Eqs. (23) and (24) is largely arbitrary. However, it is preferable to

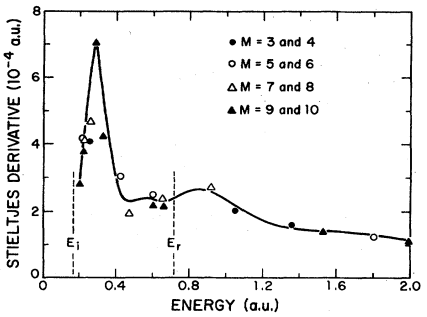

FIG. 2. Contributions to the Stieltjes derivative for $He(2^3S)+Na$ at $R=6a_0$ from various moments and least-squares fit (solid curve). E_r and E_i are the "resonance" and ionization threshold energies, respectively, at $R=6a_0$.

make a choice that avoids the occurrence of very small values of $|\epsilon_n|$, which would lead to excessive weighting of the corresponding terms in Eq. (24), and that avoids changes in the sign of ϵ_n at some point in the spectrum.[25] For the present application, the energy is referred to the ground state of NaHe at each internuclear separation. The usefulness of the moments $\tilde{S}(-k)$ lies in the fact that a new "smoothed spectrum" of values $\{\bar{\gamma}_n, \bar{\epsilon}_n\}$ for $n=1,\ldots,M$ may be obtained by inverting a small subset of the moments, up to $k=2M$. The smoothed spectrum may be shown to provide an adequate quadrature for the "cumulative function," which in our case is the energy integral of the width

$$I(\epsilon)=\int_{\epsilon_0}^{\epsilon}\Gamma(\epsilon')d\epsilon' . \tag{25}$$

Thus, a histogram approximation to $I(\epsilon)$, using the smoothed spectrum, is simply

$$\tilde{I}(\epsilon)=\sum_{n=1}^{m}\bar{\gamma}_n , \quad \bar{\epsilon}_m<\epsilon<\bar{\epsilon}_{m+1} \tag{26}$$

and the Stieltjes derivative of $\tilde{I}(\epsilon)$, defined by

$$\tilde{\Gamma}(\bar{\epsilon}_m)=\frac{\bar{\gamma}_m+\bar{\gamma}_{M+1}}{2(\bar{\epsilon}_{m+1}-\bar{\epsilon}_m)} , \quad m=1,2,\ldots \tag{27}$$

gives an approximation to the width, according to Eq. (25). Since the width is required at the resonance energy ϵ_r, some interpolation is necessary. In the present work, we use a least-squares cubic-spline fit. In Fig. 2 the calculated Stieltjes derivatives $\tilde{\Gamma}(\epsilon_m)$ from Eq. (27) and the final curve fit are illustrated for $He(2^3S)+Na$ at $R=6a_0$ and for four choices of M in the determination of the smoothed spectrum. In this example, the resonance energy is $\epsilon_r=0.7$ a.u. (relative to the ground state of NaHe). The widths in the vicinity of ϵ_r are seen to be nearly independent of M, as they should be if the procedure is converged. The comparison for $He(2^1S)+Na$ is similar. The final widths for both $He(2^{1,3}S)+Na$ are given in Fig. 3 as a function of R; in each case, the width is evaluated at the resonance energy $\epsilon_r(R)$. As expected from orbital overlap considerations, at large R the widths decrease exponentially.

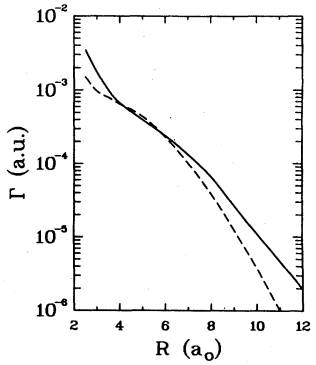

FIG. 3. Autoionization widths for $He(2^3S)+Na$ (solid curve) and $He(2^1S)+Na$ (dashed curve).

IV. PENNING-IONIZATION CROSS SECTIONS

The optical potentials defined by Eq. (14) in terms of the real potentials $V(R)$ of Fig. 1 and widths $\Gamma(R)$ of Fig. 3 were used in the Jeffreys-Wentzel-Kramers-Brillouin (JWKB) approximation to calculate the complex phase shifts which give the total Penning-ionization cross sections according to Eq. (16). The cross sections for both $He(2^{1,3}S)+Na$ are illustrated in Fig. 4 as functions of center-of-mass energy E in the range $0.01\leq E\leq 1.0$ eV. Experimental results are also shown for comparison. For $He(2^3S)$, an experimental average cross section of $(33\pm6)\times10^{-16}$ cm^2 is derived from the measured ionization rate constant (at $T=441$ K) of $(5.1\pm1.0)\times10^{-10}$ cm^3/sec in the stationary-afterglow experiment of Johnson *et al.*[14] Earlier thermal-beam measurements carried out by Hotop and Niehaus[20] originally gave a cross section for $He(2^3S)$ of 14×10^{-16} cm^2 ($+100\%$, -50%). However, recent knowledge has led them to increase their estimate of the relative collision energy to 50 ±10 meV, and the $He(2^3S)$ cross section to 24×10^{-16} cm^2 ($\pm100\%$).[26] Similarly, their revised estimate of the $He(2^1S)$ cross section is 60×10^{-16} cm^2 ($\pm100\%$); and the corresponding singlet-to-triplet ratio is now approximately 2.5. Our calculated cross sections are seen to fall

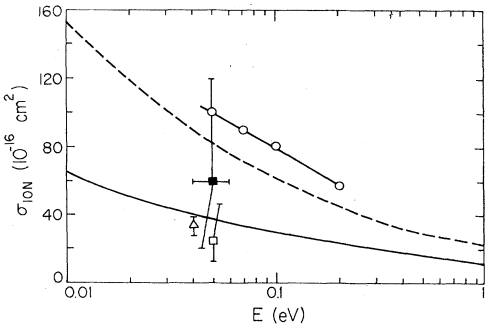

FIG. 4. Penning-ionization cross sections. Present theory for $He(2^3S)+Na$ (solid curve) and $He(2^1S)+Na$ (dashed curve). Experimental results for $He(2^3S)+Na$: □, Hotop and Niehaus (Refs. 20 and 26); △, Johnson *et al.* (Ref. 14). Experimental results for $He(2^1S)+Na$: ■, Hotop and Niehaus (Refs. 20 and 26); —○—, Haberland and Weber (Ref. 27).

within the uncertainties in the measurements. The calculated singlet-to-triplet ratio is 2.2 at 50 meV, in good agreement with the experimental value of 2.5. Haberland and Weber[27] have indirectly obtained He(2^1S) cross sections over a range of energies by a semiempirical determination of the optical potential from fits to their measured elastic differential cross sections for He(2^1S) on Na. The authors note uncertainties in determination of the optical potential, but do not quote specific uncertainties for the cross sections. The energy dependence of their cross sections is similar to that of the calculated cross sections reported here. In the calculation of the PI cross sections shown in Fig. 4, we use the modified potential curves given by Eqs. (18) and (19). The van der Waals attractive R^{-6} tail pulls in a larger number of partial waves, each of which contributes to the ionization cross section, the sensitivity being greatest at lower energies. For example, at $E_{\text{c.m.}}=0.04$ eV, setting $C_6=0$ in Eq. (18) causes reductions of 17% and 37% in the respective cross sections of He(2^3S) and He(2^1S) and the corresponding singlet-to-triplet ratio is decreased by 27%. Our results are, of course, less sensitive to precisely how the van der Waals interaction is included. For example, if the parameter R_0 in Eq. (19) is arbitrarily shifted outward by $2a_0$, i.e., to $8.27a_0$ and $10.22a_0$ for He(2^3S) and He(2^1S), respectively, the He(2^1S) cross section is reduced by 11% and that for He(2^3S) is *increased* by 3%. The latter increase in cross section is somewhat surprising since the real potential is

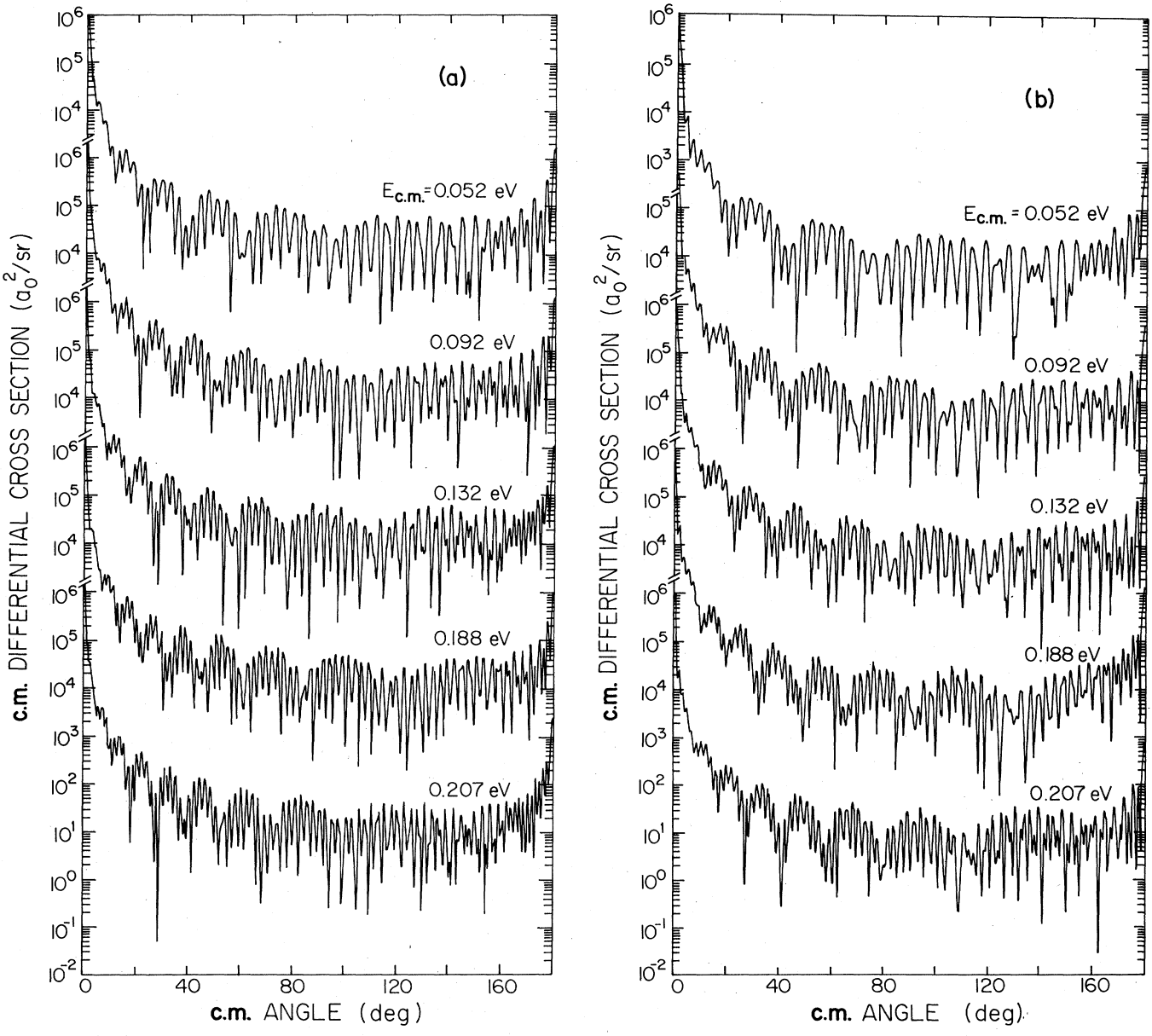

FIG. 5. Differential elastic cross sections for He(2^1S)+Na in the center-of-mass system, calculated with different potential curves: (a) potential curve corresponding to present theory, as illustrated in Fig. 1; (b) empirical potential curve of Haberland and Weber (Ref. 27).

certainly less attractive. However, there is a competing velocity effect that is important here. For a given partial wave, a deeper potential implies a higher "local" (classical) velocity and, therefore, less time for ionization to occur. This effect is always present, but is particularly evident in this comparison of He(2^3S) cross sections. As R_0 is shifted still further out to $12a_0$, the He(2^1S) cross section is reduced by 22% and the He(2^3S) cross section by 4% compared with the original choices of R_0. Finally, setting $R_0=\infty$ is, of course, equivalent to setting $C_6=0$. These comparisons give some indication of the sensitivity of the calculations to modifications of the potential curves. We believe the potentials described in Eqs. (18) and (19), with the semiempirical choices of R_0, are the most appropriate choices; we therefore consider the cross sections of Fig. 4 to be the best theoretical estimates.

It is difficult to estimate the accuracy of the width since, to the best of our knowledge, the Stieltjes method has never before been applied to any Penning-ionization process, and there are no examples of theoretical determinations of widths for PI of Na. We can quote uncertainties in the widths related to convergence of the Stieltjes procedure itself. By comparing the widths $\tilde{\Gamma}(\epsilon_r)$, at the resonance energy, corresponding to reasonable choices of the order M (e.g., $8\leq M\leq 14$) of the Stieltjes inversion, we estimate the uncertainty in the widths to be $\pm 10\%$ for both He(2^3S) and He(2^1S) states. These uncertainties correspond to about $\pm 5\%$ uncertainties in the PI cross sections at thermal energies.

V. DIFFERENTIAL ELASTIC He(2^1S)+Na CROSS SECTIONS

The recent measurements by Haberland and Weber[27] of the differential elastic cross sections for collisions between He(2^1S) and Na atoms provide some opportunity to evaluate the potential curve used in the He(2^1S) PI calculations. Unfortunately, because of the difficulty in making a Na beam, the velocity resolution in the experiment is poor ($\pm 25\%$) and most of the structure is washed out. Nevertheless, a qualitative comparison is possible. We believe that it is most informative to compare the center-of-mass, differential cross sections calculated with our potential (shown in Fig. 1) with those calculated with the empirical potential of Haberland and Weber. This comparison is made in Fig. 5 at the c.m. energies where the experiment was done. The empirical potential was chosen by Haberland and Weber such that the corresponding differential cross section, when transformed to be laboratory system and averaged with respect to experimental beam and detector conditions (not completely specified in their paper), is in good agreement with the measurements. However, the choice is not unique and their analytic form (hybridized Morse potential) does not have the correct asymptotic form. Hence the results obtained at small angles with our potential should be better. Also, the repulsive wall of the empirical potential is rather uncertain since the influence of the width $\Gamma(R)$ is greatest there. Haberland and Weber use a simple exponential form for $\Gamma(R)$, which is similar to our *ab initio* result at $R>R_e$, but is much larger at small R. The repulsive part of the potential mainly affects large-angle scattering. In spite of these uncertainties, it can be seen in Fig. 5 that the c.m. differential cross sections calculated with the two potentials are similar in shape except at very small angles. On the other hand, the magnitudes of the differential cross sections calculated with our potential are substantially greater than those calculated with the empirical potential at all angles—the experimental measurements themselves are not absolute. This difference is due primarily to the difference in the long-range forms of the potentials and secondarily to the difference in ionization widths.

Although the theoretical information content is somewhat less accessible and the results depend on the detailed experimental conditions, it is also interesting to consider one example of the differential cross section in the laboratory system. We do this in Fig. 6 for the results corresponding to $E_{\text{c.m.}}=0.052$ eV at $0°\leq\theta_{\text{lab}}\leq 180°$. The beam velocities appropriate to the Haberland and Weber experiment have been used, but averaging over velocity and angle, which would eliminate most of the structure, has not been performed. The pronounced peak at $\theta_{\text{lab}}=104°$ is a result of glory scattering and was observed in the experiment done at $E_{\text{c.m.}}=0.052$ eV. It was not seen experimentally at higher c.m. energies since it then occurs at

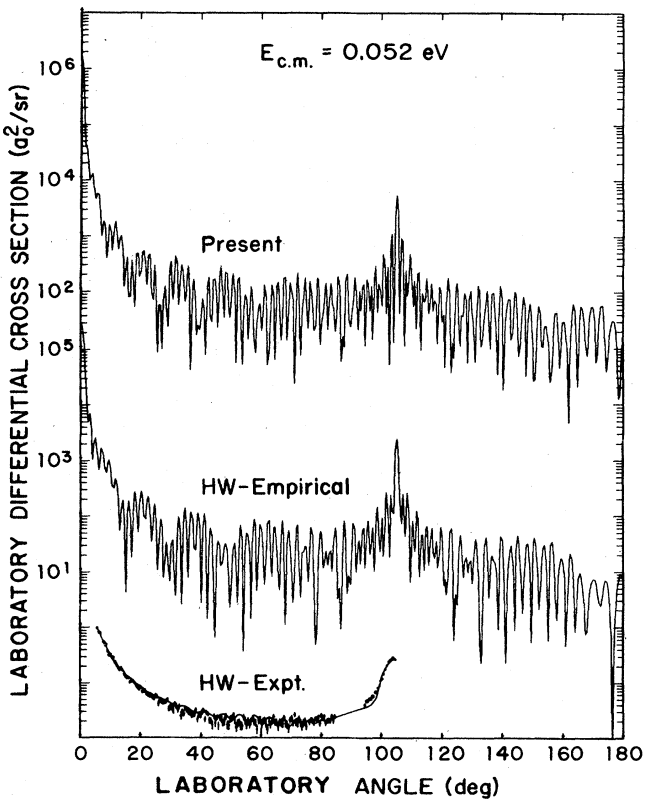

FIG. 6. Differential elastic cross sections for He(2^1S)+Na in the laboratory system at an energy corresponding to $E_{\text{c.m.}}=0.052$ eV. The cross section calculated with the present potential (see Fig. 1) is compared with that calculated using the empirical potential of Haberland and Weber (HW) (note change in scale) and with their actual experimental measurements (in arbitrary units).

laboratory angles larger than detected. This peak is of purely kinematic origin, corresponding to $\theta_{\text{c.m.}} = 180°$, and so, as Haberland and Weber point out, its angular position gives no information about the potential.

The differential cross sections shown in Figs. 5 and 6 are suggestive of the resolution that would be required to obtain a more rigorous test of the theoretical potential curves. However, it appears that obtaining the real and imaginary parts of the potential from differential elastic scattering data will require high precision unless one of them is already known accurately from another source. Test calculations done with $\Gamma(R)$ set to zero show that the overall periodicity of the interference structure is not much changed, but that the width does have an observable effect on the detailed structure of particular peaks as well as on the magnitudes.

ACKNOWLEDGMENTS

We would like to thank Dr. R. T Pack for helpful discussions of the differential cross sections, and Dr. H. Haberland and Dr. H. Hotop for additional information about the experimental results. One of the authors (N.F.L.) wishes to acknowledge partial support for this work by the U.S. Department of Energy (Office of Basic Energy Sciences) and by the Robert A. Welch Foundation. This work was performed under the auspices of the U.S. Department of Energy.

[1]N. F. Mott and H. S. W. Massey, *The Theory of Atomic Collisions,* 3rd ed. (Clarendon, Oxford, 1965), Chap. 19, p. 609.
[2]H. S. W. Massey, *Electronic and Ionic Impact Phenomena* (Oxford University, London, 1971), Vol. III, p. 1914.
[3]H. S. W. Massey, *Electronic and Ionic Impact Phenomena,* Ref. 2, p. 1810.
[4]B. M. Smirnov, Usp. Fiz. Nauk **133**, 569 (1981) [Sov. Phys.—Usp. **24**, 251 (1981)].
[5]H. Hotop, Radiat. Res. **59**, 379 (1974).
[6]A. Niehaus, in *The Excited State in Chemical Physics,* Vol. 45 of *Advances in Chemical Physics,* edited by J. W. McGowan (Wiley-Interscience, New York, 1981), p. 399; and in *Physics of Electronic and Atomic Collisions,* edited by S. Datz (North-Holland, Amsterdam, 1982), p. 237.
[7]H. Nakamura, J. Phys. Soc. Jpn. **26**, 1473 (1969).
[8]W. H. Miller, J. Chem. Phys. **52**, 3563 (1970); Chem. Phys. Lett. **4**, 627 (1970).
[9]R. J. Bieniek, Phys. Rev. A **18**, 392 (1978).
[10]W. H. Miller and H. F. Schaefer, J. Chem. Phys. **53**, 1421 (1970); W. H. Miller, C. A. Slocomb, and H. F. Schaefer, *ibid.* **56**, 1347 (1972); A. P. Hickman and H. Morgner, J. Phys. B **9**, 1765 (1976); J. Chem. Phys. **67**, 5484 (1977).
[11]A. D. Isaacson, J. Chem. Phys. **71**, 180 (1979).
[12]A. P. Hickman, A. D. Isaacson, and W. H. Miller, J. Chem. Phys. **66**, 1483 (1977).
[13]J. S. Cohen and N. F. Lane, J. Chem. Phys. **66**, 586 (1977).
[14]C. E. Johnson, C. A. Tipton, and H. G. Robinson, J. Phys. B **11**, 927 (1978).
[15]Y. A. Tolmachev and D. Fogel, Opt. Spektrosk. **48**, 818 (1980) [Opt. Spectrosc. (USSR) **48**, 451 (1980)].
[16]T. F. O'Malley, Phys. Rev. **150**, 14 (1966).
[17]H. Feshbach, Ann. Phys. (N.Y.) **5**, 357 (1958); **19**, 287 (1962).
[18]W. H. Miller, Chem. Phys. Lett. **4**, 627 (1970).
[19]The even-tempered expansions were guided by Huzinaga's primitive sets. See S. Huzinaga, J. Chem. Phys. **42**, 1293 (1965); S. Huzinaga and Y. Sakai, *ibid.* **50**, 1371 (1969).
[20]H. Hotop and A. Niehaus, Z. Phys. **238**, 452 (1970).
[21]A. Dalgarno and G. A. Victor, J. Chem. Phys. **49**, 1982 (1968).
[22]A. U. Hazi, J. Phys. B **11**, L259 (1978).
[23]P. W. Langhoff, Chem. Phys. Lett. **22**, 60 (1973); and in *Electron and Photon Molecule Collisions,* edited by T. Rescigno, V. McKoy, and B. Schneider (Plenum, New York, 1979), p. 183.
[24]W. P. Reinhardt, in *Theory and Applications of Moment Methods in Many-Fermion Systems,* edited by B. J. Dalton, S. M. Grimes, J. P. Vary, and S. A. Williams (Plenum, New York, 1980), p. 129.
[25]R. L. Martin, W. R. Daasch, and E. R. Davidson, J. Chem. Phys. **71**, 2375 (1979); J. S. Cohen, R. L. Martin, and W. R. Wadt, Phys. Rev. A **24**, 33 (1981).
[26]H. Hotop (private communication); also see discussion in Ref. 27.
[27]H. Haberland and W. Weber, J. Phys. B **13**, 4147 (1980).